THIRTEENTH EUROPEAN ROTORCRAFT FORUM

62
Paper No. 7

An Experimental and Analytical Investigation of Stall Effects on Flap-Lag Stability in Forward Flight

J. Nagabhushanam
Dept. of Aeorspace Engineering
Indian Institute of Science
Bangalore 560 012
India

Gopal H. Gaonkar
Dept. of Mechanical Engineering
Florida Atlantic University
Boca Raton, FL 33431-0991
U.S.A.

Michael J. McNulty
Aeroflightdynamics Directorate
U.S. Army Aviation Research & Technology Activity (AVSCOM)
Moffett Field, CA, 94035-1099
U.S.A.

September 8-11, 1987

Arles, France

ASSOCIATION AERONAUTIQUE ET ASTRONAUTIQUE DE FRANCE

AN EXPERIMENTAL AND ANALYTICAL INVESTIGATION OF STALL EFFECTS ON FLAP-LAG STABILITY IN FORWARD FLIGHT

J. Nagabhushanam,
Indian Institute of Science
Department of Aerospace Engring
Bangalore 560 012, INDIA

Gopal H. Gaonkar
Florida Atlantic University
Dept. of Mechanical Engineering
Boca Raton, FL 33431-0991, U.S.A.

Michael.J. McNulty
Aeroflightdynamics Directorate
U.S. Army Aviation Res. & Tech. Activity
Moffett Field, CA 94035-1099, U.S.A.

ABSTRACT

Experiments have been performed with a 1.62m diameter hingeless rotor in a wind tunnel to investigate flap-lag stability of isolated rotors in forward flight. The three-bladed rotor model closely approaches the simple theoretical concept of a hingeless rotor as a set of rigid, articulated flap-lag blades with offset and spring restrained flap and lag hinges. Lag regressing mode stability data was obtained for advance ratios as high as 0.55 for various combinations of collective pitch and shaft angle. The prediction includes quasi-steady stall effects on rotor trim and Floquet stability analyses. Correlation between data and prediction is presented and is compared with that of an earlier study based on a linear theory without stall effects. While the results with stall effects show marked differences from the linear theory results, the stall theory still falls short of adequate agreement with the experimental data.

NOMENCLATURE

a	Linear lift curve slope
c	Blade chord
$c_l(\alpha)$	Lift coefficient at α
$c_d(\alpha)$	Drag coefficient at α
c_{l_o}	Lift coefficient at $\bar{\alpha}$
c_{d_o}	Drag coefficient at $\bar{\alpha}$
$c_{l_{\alpha o}}$	Slope of the lift-coefficient curve at $\bar{\alpha}$

$c_{d\alpha o}$	Slope of the drag-coefficient curve at $\bar{\alpha}$
d	Drag force per unit length of the blade
e	Hinge offset/R
F_{yk}	Force per unit length of the k-th blade in the plane of rotation
F_{zk}	Force per unit length of the k-th blade in the plane perpendicular to the plane of rotation
I	Blade moment of inertia
l	Lift force per unit length of blade
$p_1, p_2, \cdot\cdot, p_{10}$	Coefficients as defined in equation (13)
R	Rotor blade radius or flap-lag structural coupling parameter
r	Spanwise station from hinge
U	Resultant flow velocity at a blade section/(ΩR)
U_P	Transverse velocity component/(ΩR)
U_T	Tangential velocity component/(ΩR)
U_{Po}	Trim-state transverse velocity component/(ΩR)
U_{To}	Trim-state tangential velocity component/(ΩR)
α	Blade section angle of attack
$\bar{\alpha}$	Trim-state blade section angle of attack
α_s	Shaft-tilt or shaft angle
β	Flapping angle of the blade
γ	Lock number, $\rho a c R^4/I$
ζ	Lead-lag angle of the blade
ΔU_P	Perturbed transverse velocity component/(ΩR)
ΔU_T	Perturbed tangential velocity component/(ΩR)
$\Delta\alpha$	Incremental angle of attack, $\alpha-\bar{\alpha}$
θ_0	Collective blade pitch
ϕ	Local inflow angle
$\bar{\phi}$	$\mathrm{Tan}^{-1}(U_{Po}/U_{To})$
ϕ_o	U_{Po}/U_{To}
ρ	Air density
Ω	Rotor speed
ω_ζ	Dimensionless rotating lag frequency/Ω
λ	Total inflow ratio, $\lambda_i + \mu \tan\alpha_s$
λ_i	Induced flow due to thrust
μ	Advanced ratio
ψ_k	Azimuth angle of the k-th blade

$(\dot{})$ $\quad \frac{d}{d\psi}( )$

INTRODUCTION

In an earlier study[1] we presented a correlation between data and prediction for flap-lag stability in forward flight. The correlation was based on a comprehensive data base on the lag regressing mode damping of an isolated rotor with three blades. Virtually rigid flap-lag blades were used, and the data base included aerodynamically demanding test cases with advance ratio, μ, as high as 0.55 and shaft-tilt angle, α_s, as high as 20°. The prediction was based on a linear quasi-steady aerodynamics theory with dynamic inflow. Overall, the prediction was found to be adequate for very low values of collective pitch, but deteriorated at the higher pitch angles. References 2 and 3, though restricted to hovering conditions, showed that inclusion of quasi-steady, nonlinear airfoil characteristics (stall effects) significantly improves correlation. The purpose of this continuing study is to investigate the effects of nonlinear airfoil characteristics under more demanding forward flight conditions.

In forward flight the number of correlation studies based on models that are intentionally simplified to isolate one aspect of the overall rotor stability problem are limited. Specifically stated, the structural simplicity of a rigid blade model facilitates isolation of aerodynamic effects. For an improved picture of airfoil effects, we now investigate the effects of nonlinear local lift, of nonlinear local drag and of profile drag at zero angle of attack. Furthermore, the correlation includes different combinations of pitch settings $(o \le \theta_o \le 8°)$, advance ratios $(o \le \mu \le o{\cdot}55)$ and shaft-tilt angles $(o \le \alpha_s \le 20°)$ and thus provides a range of rotor loading conditions in forward flight.

EXPERIMENT AND DATA

For completeness, we include a brief account of the experimental model, for details see reference 1. To ensure the validity of using a simple flap-lag analysis for correlations, the three-bladed rotor used flexures to simulate articulated blades with spring restraint and coincident flap and lag hinges. The effective hinge offset was 0.11R. The blades were stiff relative to the flap and lag flexures so that the first flap and lag modes essentially involve only rigid body blade motions. Further, the design insures a rotating first

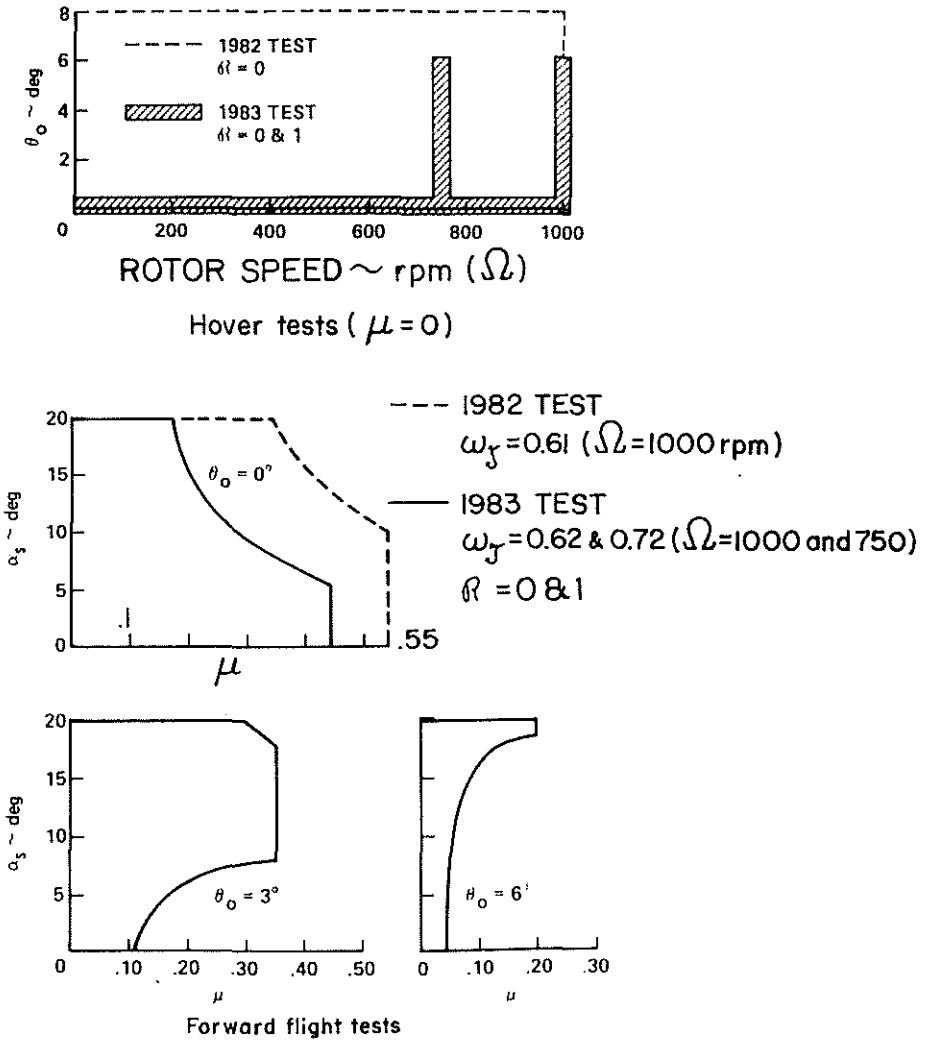

Figure 1b: Conditions tested

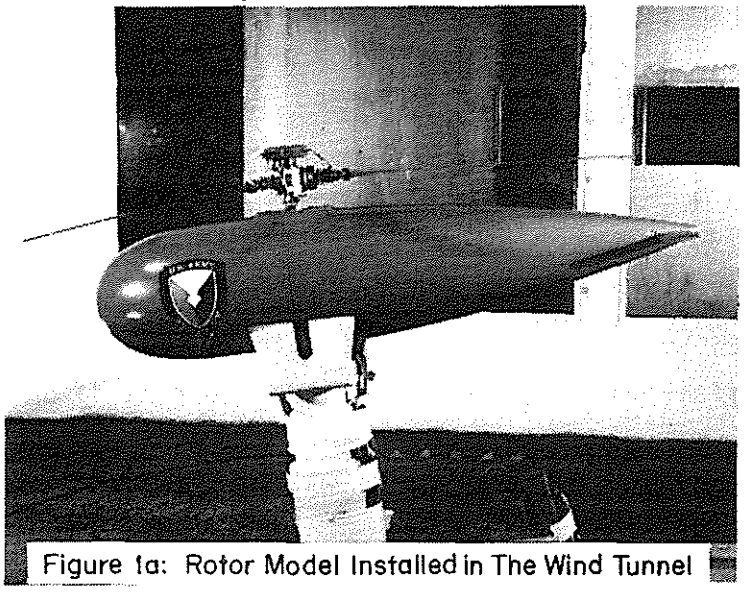

Figure 1a: Rotor Model Installed in The Wind Tunnel

Figure 1: Rotor Model Installed in The Wind Tunnel, and Hovering and Forward Flight Conditions Tested.

torsional frequency of at least 9/Rev over the entire rotor speed range tested, and thus virtually eliminating the need to consider a torsional degree of freedom. The measured and assumed parameter values of the test model are given in table 1.

The model tested was a 1.62m diameter three-bladed hingeless rotor mounted on a very stiff rotor stand so that the stability data was representative of an isolated rotor, see Fig. 1a. The rotor had no cyclic-pitch control and collective pitch was set manually prior to each run. At a given advance ratio, rotor speed and collective pitch the shaft tilt was the only means of controlling the rotor. Thus the rotor was operated untrimmed with an unrestricted tilt of the tip-path plane. The model was shaken in roll to excite the lag modes, and was then locked up and the transient response recorded. The frequency and damping data were then obtained from the time histories via the moving block technique. In forward flight two rotor speeds were used (Ω = 750 and 1000 rpm) corresponding to ω_ζ values of 0.62 and 0.72. Advance ratio, shaft-tilt angle and collective pitch were varied to cover the test envelope shown in figure 1b. At each condition tested at least two separate damping measurements were obtained.

Table 1: Model Properties

Number of blades	3
Radius	0.81 m
Chord	0.0419 m
Airfoil section	NACA 23012
Lift curve slope a	5.73
Profile drag coefficient at zero angle of attack (assumed)	0.0079 and 0.012
Nondimensional hinge offset	0.111
Blade inertia about hinge	0.01695 kg-m^2
Blade mass center distance from hinge	0.188m
Blade mass (Outboard of hinge)	0.204 kg
Nonrotating flap frequency	3.09 Hz
Nonrotating lead-lag frequency	7.02 Hz
Average lead-lag structural damping ratio	0.185% critical
Lock number γ (based on a=5.73)	7.54

ANALYSIS

The analytical model consists of an articulated rigid-blade flap-lag model with flap and lag spring restraints at the offset hinge. The hinge offset of 11.1% in flap and lag is accounted for in both the rotor trim and stability analyses. The rotor used no cyclic pitch so that at a given advance ratio, the collective pitch and the shaft tilt angles are the known trim parameters. The analytical model has the capability to include stall effects in both the rotor trim (zero cyclic pitch, and cyclic flapping present) and Floquet stability analyses. At an azimuth angle ψ_k, we consider a blade element of length dr of the k-th blade. The corresponding resultant flow velocity U and inflow angle ϕ in terms of normal and tangential velocity components are given by

$$U = \sqrt{U_T^2 + U_P^2} \approx U_T(1+\tfrac{1}{2}U_P^2/U_T^2) \tag{1}$$

$$\phi = \tan^{-1}U_P/U_T \tag{2}$$

The force components parallel and perpendicular to the plane of rotation are as follows:

$$dF_{yk} = (-l \sin \phi - d \cos \phi)dr \tag{3(a)}$$

$$dF_{zk} = (l \cos \phi - d \sin \phi)dr \tag{3(b)}$$

where

$$l = \tfrac{1}{2}\rho c\Omega^2R^2U^2c_l(\alpha) \tag{4(a)}$$

$$d = \tfrac{1}{2}\rho c\Omega^2R^2U^2c_d(\alpha) \tag{4(b)}$$

For a pitch setting θ_0 and trim angle of attack $\bar{\alpha}$, we have

$$\alpha = \theta_0 - \phi \text{ and } \bar{\alpha} = \theta_0 - \bar{\phi} \tag{6}$$

where

$$\bar{\phi} = \tan^{-1} U_{P0}/U_{T0} \tag{7}$$

The perturbation angle of attack $\Delta\alpha$ about $\bar{\alpha}$ is expressed as

$$\alpha - \bar{\alpha} = \Delta\alpha = \bar{\phi} - \phi \tag{8}$$

$$\approx \phi_0 - \frac{\phi_0^3}{3} - \frac{U_P}{U_T} + \frac{U_P^3}{3U_T^3}$$

Expanding $c_l(\alpha)$ and $c_d(\alpha)$ about $\bar{\alpha}$ we get

$$c_l(\alpha) = c_l(\bar{\alpha}) + (\frac{dc_l}{d\alpha})_{\bar{\alpha}} \quad (\alpha - \bar{\alpha}) \tag{9a}$$

$$c_d(\alpha) = c_d(\bar{\alpha}) + (\frac{dc_d}{d\alpha})_{\bar{\alpha}} \quad (\alpha - \bar{\alpha}) \tag{9b}$$

Similarly substituting equations 1, 4 and 9 in equation 3, we get

$$dF_{yk} = \tfrac{1}{2}\rho c R^2 \Omega^2 U\{ - (c_{do} + c_{d\alpha o}\Delta\alpha)\, U_T - (c_{lo} + c_{l\alpha o}\Delta\alpha) U_P\} dr \tag{10a}$$

$$dF_{zk} = \tfrac{1}{2}\rho c R^2 \Omega^2 U\{ - (c_{do} + c_{d\alpha o}\Delta\alpha)\, U_P + (c_{lo} + c_{l\alpha o}\Delta\alpha)\, U_T\} dr \tag{10b}$$

where

$$U_P = e \cos\zeta + \cos\beta\ (1 + \dot{\zeta}) r/R + \mu \sin(\psi + \zeta) \tag{11}$$

$$U_T = e \sin\zeta \sin\beta + r\dot{\beta}/R + \lambda \cos\beta + \mu \sin\beta \cos(\psi + \zeta)$$

Now we perturb the total velocity component about the trim state. That is

$$U_P = U_{Po} + \Delta U_T \tag{12}$$

$$U_T = U_{To} + \Delta U_T$$

Substituting equations 1, 8 and 12 in equation 10 and neglecting the products of perturbation quantities such as ΔU_T^2, we get

$$dF_{yk} = \tfrac{1}{2}\rho c \Omega^2 R^2 U\{ p_1 U_T^2 + p_2 U_T U_P + p_3 U_P^2 + p_4 U_P \Delta U_P + p_5 U_P \Delta U_T\} dr, \tag{12a}$$

$$dF_{zk} = \tfrac{1}{2}\rho c \Omega^2 R^2 U\{p_6 U_T^2 + p_7 U_T U_P + p_8 U_P^2 + p_9 U_P \Delta U_P + p_{10} U_P \Delta U_T\} dr, \tag{12b}$$

where

$$p_1 = \{ - c_{do} - c_{d\alpha o}(\phi_o - \frac{\phi_o^3}{3}) \} \tag{13}$$

$$p_2 = \{ c_{d\alpha o} - c_{lo} - c_{l\alpha o}(\phi_o - \frac{\phi_o^3}{3}) \}$$

$$p_3 = \{ - 1/2\ c_{do} - \frac{c_{d\alpha o}\phi_o}{3} - 1/2\ \phi_o c_{lo} + c_{l\alpha o}(1 - \frac{\phi_o^3}{3}) \}$$

$$p_4 = \{ c_{d\alpha o}\ (1/6\ \phi_o - 1/2\ \phi_o^3) - 1/2\ \phi_o c_{lo} - c_{l\alpha o}\ \frac{\phi_o^2}{6} \}$$

$$p_5 = \{ - \frac{c_{d\alpha o}\,\phi_o^2}{6} + c_{lo}\,\frac{\phi_o^2}{2} + \frac{1}{6}\,c_{l\alpha o}\phi_o^3 \}$$

$$p_6 = \{ c_{lo} + c_{l\alpha o}(\phi_o - \frac{1}{3}\,\phi_o^3) \}$$

$$p_7 = \{ - c_{l\alpha o} - c_{do} - c_{d\alpha o}\,(\phi_o - \frac{1}{3}\phi_o^3) \}$$

$$p_8 = \{ \frac{c_{lo}}{2} + \frac{c_{l\alpha o}\phi_o}{3} - \frac{c_{do}\phi_o}{2} + c_{d\alpha o}\,(1 - \frac{1}{3}\,\phi_o^3\,) \}$$

$$p_9 = \{ - c_{l\alpha o}(1/6 - \frac{\phi_o^3}{3}) - \frac{c_{do}\phi_o}{2} - \frac{c_{d\alpha o}\phi_o^2}{6} \}$$

$$p_{10} = \{ \frac{c_{l\alpha o}\phi_o^2}{6} - \frac{c_{do}\phi_o^2}{2} + \frac{c_{d\alpha o}\phi_o^3}{6} \}$$

We observe that the quantities $c_{l\alpha o}$, $c_{d\alpha o}$, c_{lo} and c_{do} in p_1, p_2,..,p_{10} experience large variations in numerical values and that the derivation is carried out in terms of p_1,..,p_{10} throughout (that is without breaking the p quantities in terms of individual components). Further we stipulate that p_1....p_{10} are of order unity in deriving the equations. The subsequent derivation of the flap-lag-dynamic inflow equation follows reference 1 except for the following difference. At any azimuth station, we integrate the aerodynamic terms numerically along blade span since c_{lo}, $c_{l\alpha o}$, c_{do}, $c_{d\alpha o}$ are complex functions of radial coordinate and azimuth.

To generate the equations, we use a special purpose symbolic processor DEHIM (Dynamic Equations of Helicopter Interpretive Models).[6,7] It also generates FORTRAN coded statements of the equations which are utilized to form subroutines. These subroutines are directly linked with numerical analysis program to facilitate evaluate the coefficients of the governing equations. The numerical analysis program evaluates the rotor trim parameters with stall characteristics, performs Floquet stability analysis and identifies the modes. The numerical integration of aerodynamic terms in the equations along the span is done by a 10 point Gaussian quadrature. We generate the Floquet transistion matrix by

subroutine DVERK(IMSL) which is a Runge-Kutta-Verner fifth and sixth order method. The program evaluates the four aerofoil characteristics c_{l_0}, $c_{l_{\alpha 0}}$, c_{d_0} and $d_{d\alpha 0}$ for any given angle of attack α by linear interpolation from a table with data at 5°intervals for $0 \leq \alpha \leq 360°$. The airfoil characteristics used in this paper are shown in figure 2. For low angles of attack these are the same as the airfoil properties used in our earlier study[1] based on the linear theory except for the following difference. In reference 1, c_d ($\alpha = 0$) = 0.0079 throughout. However, in the present study we consider two values of c_d ($\alpha = 0$); 0.0079 as in references 2 and 3 and 0.012 as in references 4. With double precision arithmatic, the average CPU time for each case was about 5 minutes on VAX 750 computer.

Finally, we conclude this section with a note concerning the comparison between the numerical results from the stall theory and from the linear theory. For a consistent comparison for the entire test envelope, we compute the damping data from the stall theory and also from the same stall theory by suppressing the stall effects. The latter computations refer to the linear theory and compare with those in reference 1.

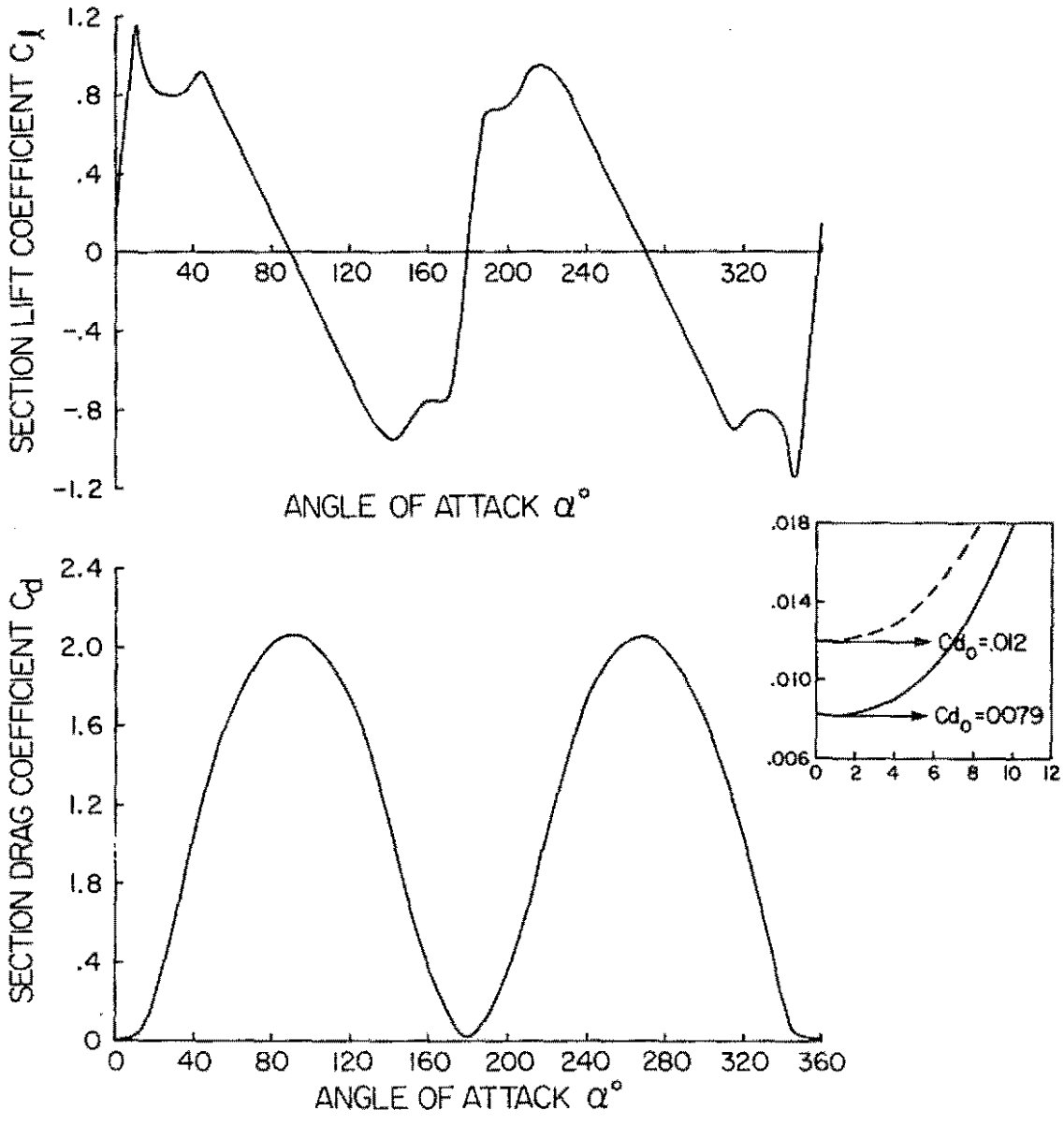

FIG. 2 ASSUMED NON-LINEAR LIFT AND DRAG CHARACTERISTICS OF AIRFOIL

RESULTS

We predict the lag regressing mode damping for the parameter values of the test model given in Table 1, covering the entire test envelope shown in figure 1b. We use two theories, the quasi-steady aerodynamics with dynamic inflow (linear theory) and the stall theory which is this linear theory refined to include nonlinear airfoil section local lift and drag characteristics in a quasi-steady manner. If not stated otherwise, the following convention and parameter values apply: full lines for predictions with linear theory, dotted lines for predictions with stall theory and c_d (α = o) = 0.0079, R = 0.0 and ω_ζ = 0.72 (Ω = 1000 rpm).

We begin the discussion of correlation with figure 3 which is for the hovering case for four values of the collective pitch setting $\theta_o{}^\circ$ = 0, 4, 6 and 8. The improvement with inclusion of quasi-steady stall is marginal and it is due to nonlinear airfoil-section local drag coefficient (non-linear drag for short) in substall. This is expected because the angle of attack is low for all the four cases tested. For example at 0.7R, the approximate mean or trim angle of attack $\bar{\alpha}$ varies from 0° for $\theta_o{}^\circ$ = 0, to 4° for $\theta_o{}^\circ$ = 8. Overall the correlation is fair. However we observe two types of consistent underpredictions. For Ω < 300 rpm, the first type is observed for which the deviation from the data essentially remains the same with increasing pitch setting. For Ω > 700 rpm, the second type is observed for which the deviation increases with increasing θ_o. These deviations were found not to be associated with ground effect, recirculation and nonuniform steady inflow.[1] The present stall theory shows that the deviations are not associated with nonlinear drag. The deviations are surprising and merit further study. (The role of dynamic inflow with stall and of higher airfoil profile drag with c_d (α= 0) = 0.012 is discussed later).

We now present the forward flight case in figure 4 which shows the correlation for zero collective and for relatively low values of the shaft-tilt angle ($\alpha_s{}^\circ \leq 6$). For $\mu \leq 0.4$, both the theories show good agreement with the data for all the four cases, $\alpha_s{}^\circ$ = 0, 2, 4, and 6. This is expected since the predictions refer to low thrust conditions due to zero pitch setting and low shaft-tilt angles. For $\mu > 0.4$ and $\alpha_s{}^\circ$ = 4 and 6, the non-linear effects begin to affect the predictions.

To facilitate further discussion, we refer to the areas of the stall regions ($|\alpha| > 12°$) based on trim values as a means of quantifying stall effects. Stall plots are given in figure 5 including different combinations of θ_o and α_s

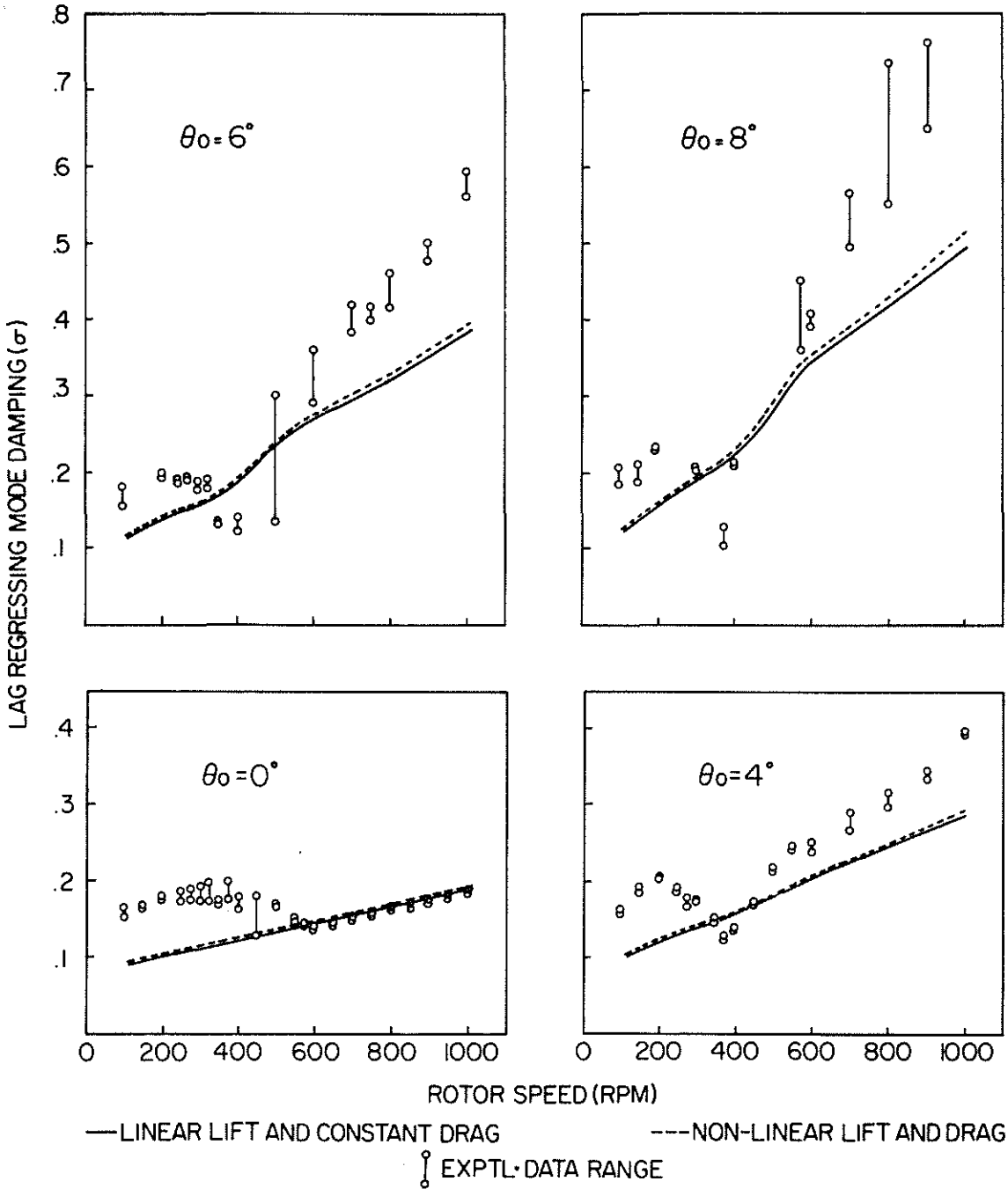

FIG.3 CORRELATION OF LAG REGRESSING MODE DAMPING WITH AND WITHOUT STALL EFFECTS IN HOVER

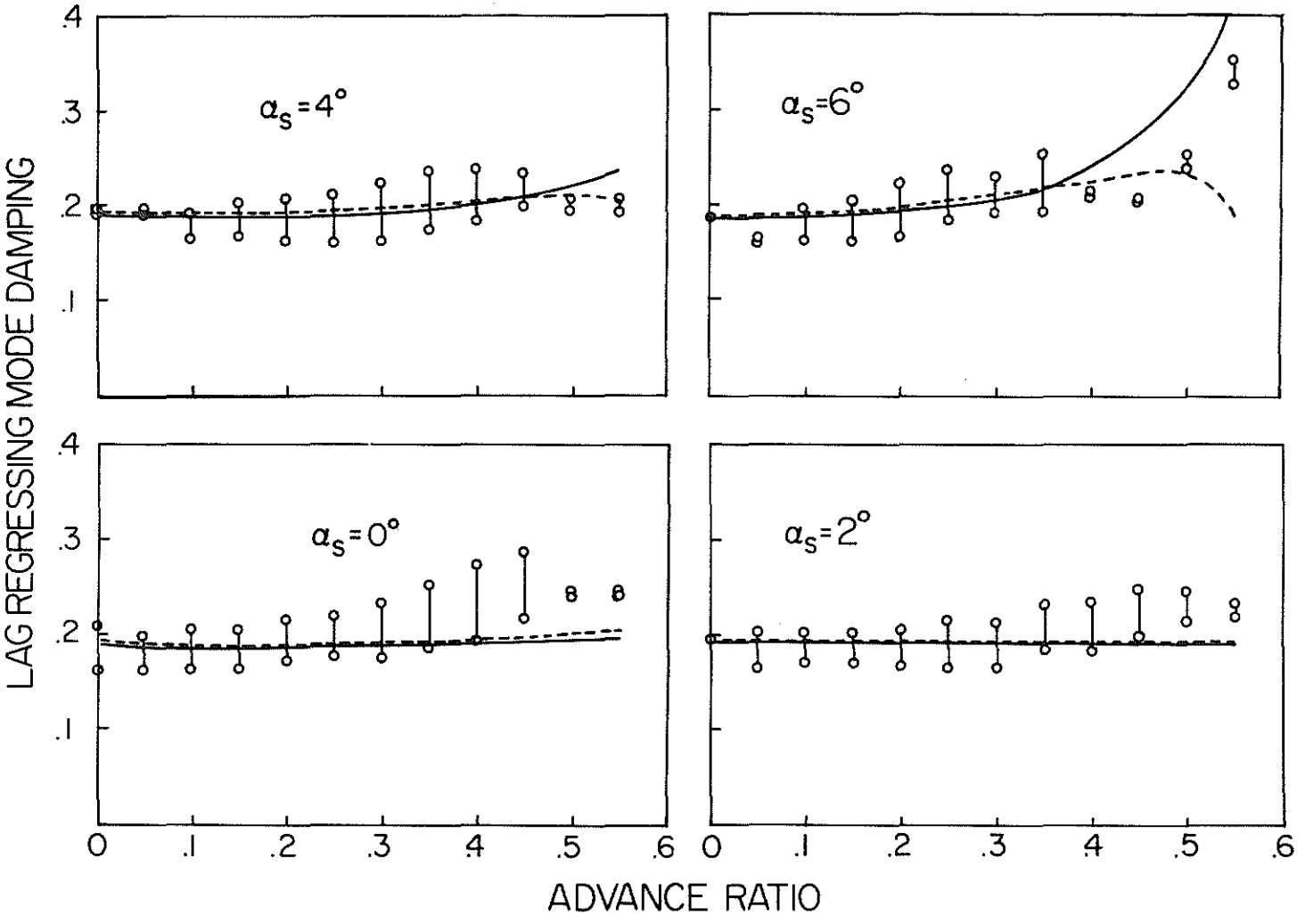

FIG. 4 CORRELATION OF LAG REGRESSING MODE DAMPING WITH AND WITHOUT STALL EFFECTS IN FORWARD FLIGHT FOR LOW SHAFT TILT ANGLES FOR $\theta_o = 0°$

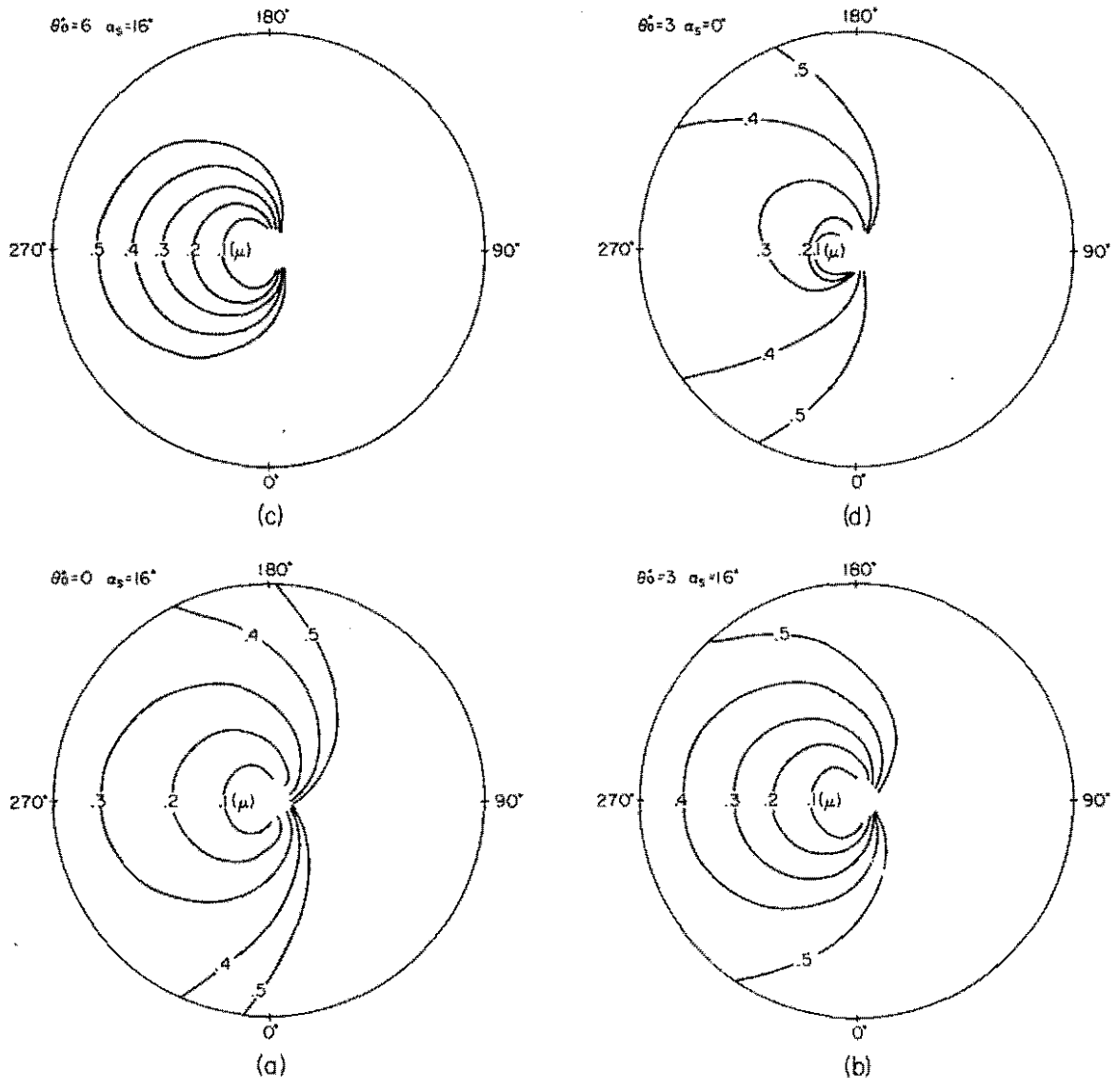

FIG.5 STALL REGIONS FOR VARIOUS ADVANCE RATIOS AND FOR $\theta_0^\circ = 0^\circ, 3^\circ$ AND 6°

for various μ values. We observe (not included in figure 5 but given reference 1) that 10% to 12% of the rotor disk is in stall for $\mu = .5$ and $\alpha_s° = 4$, and for $\mu = .4$ and $\alpha_s° = 6$, and that this percentage increases to 16-18 for $\mu = .5$ and $\alpha_s° = 6$. Overall, both the theories give good correlation. However, a qualitative aspect of the correlation merits special mention. The data point at $\mu = 0.55$ and $\alpha_s° = 6$ shows that the damping is increasing with increasing μ; a trend that is not captured by the stall theory. We should also mention that this trend is captured by the linear theory, although nearly 1/4 of the rotor disk is experiencing stall for $\mu = .55$ and $\alpha_s° = 6$.[1]

Figure 6 shows the correlation at the same zero collective pitch setting for higher values of the shaft-tilt angle ($8 \leq \alpha_s° \leq 20$) from hovering to high advance ratios ($o \leq \mu \leq .55$). Both the theories show close agreement with the data for all four cases ($\alpha_s° = 8$, 12, 16, and 20) when less than 10%-12% of the rotor disk is in stall.[1] Specifically, these ranges are: $\mu \leq .3$, $\alpha_s° = 8$; $\mu \leq .25$, $\alpha_s° = 12$; $\mu \leq .225$, $\alpha_s° = 16$, and $\mu \leq .175$, $\alpha_s° = 20$. They represent very low thrust conditions with negligible influence of nonlinear drag in substall. Moreover, the stall theory fails to capture the trend of the data (i.e., increasing damping with increasing μ) when more than 20-25% of the disk is in stall, as observed for the following ranges: $\mu > .425$, $\alpha_s° = 8$; $\mu > .325$, $\alpha_s° = 12$; $\mu > .3$, $\alpha_s° = 16$, and $\mu = 0.25$, $\alpha_s° = 20$. For the in-between cases when 12%-20% of the disk is in stall, the stall theory shows perhaps a slight improvement. Reiterating we summarize the correlations in figures 4 and 6 as follows. First, when more than about 20-25% of the disk is in stall, which occurs for high values μ and α_s, the stall theory does not capture the trend of the data. We suggest that dynamic stall may be contributing to this situation. It is not known why the linear theory gives better results here. Second, when less than about 10-12% of the disk is in stall, the stall theory is found to merge with the linear theory (low α values due to low values of pitch setting, μ and α_s). Third, between these two ranges the nonlinear theory seem to give slightly better results than the linear theory does, but this is not conclusively demonstrated by the nonlinear theory.

For the three-degree collective case, figure 7 shows the results for $0 \leq \mu \leq .55$ and $0 \leq \alpha_s° \leq 20$. The data shows the trend that the damping decreases smoothly with increasing values of μ and α_s ($\alpha_s \geq 12°$). The linear theory becomes qualitatively inaccurate with increasing μ and $\alpha_s°$ (≥ 12), showing the opposite trend of increasing damping with increasing μ. The stall theory, like the data shows an eventual damping reduction with increasing advance ratio, but the

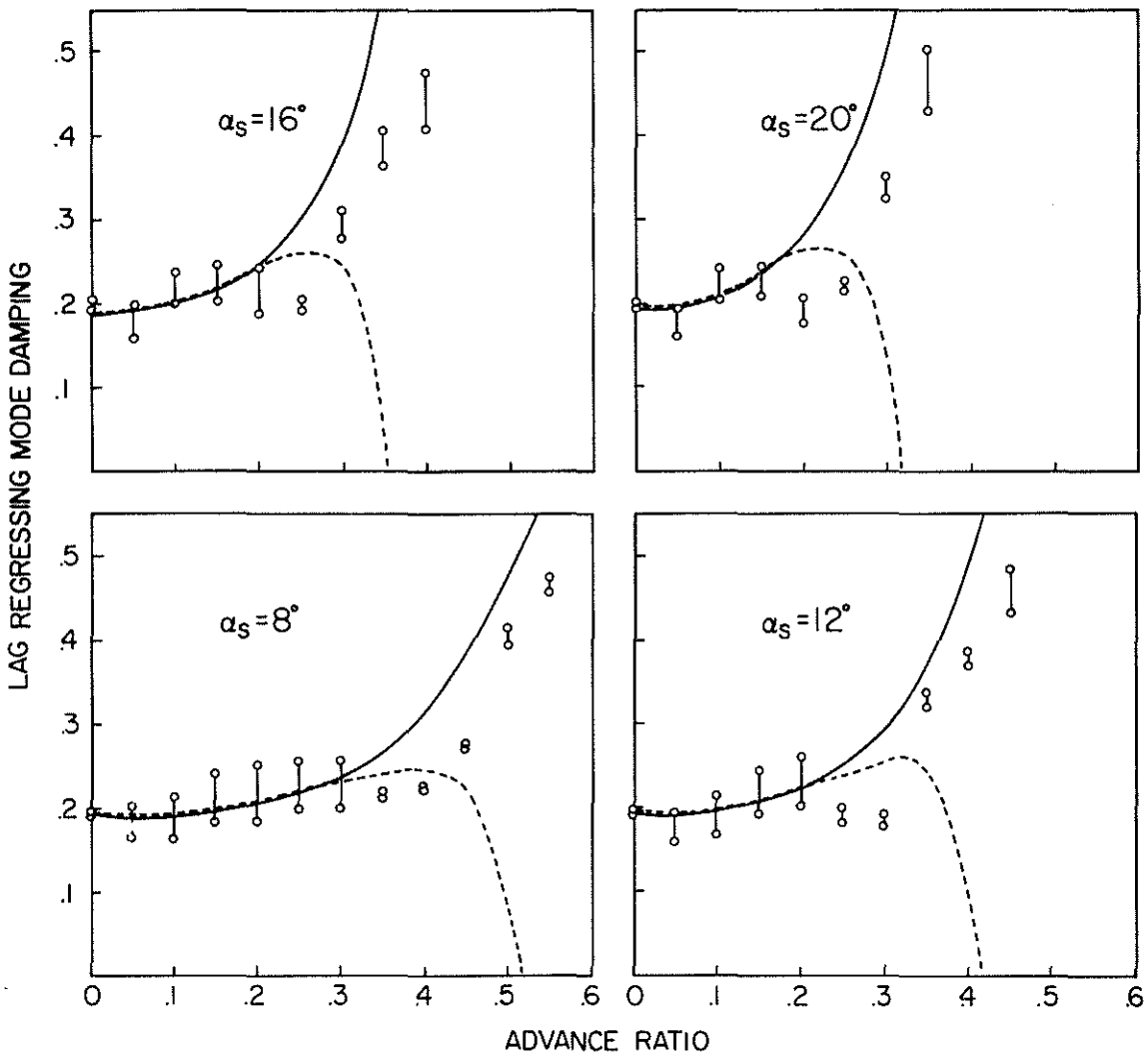

FIG.6 CORRELATION OF LAG REGRESSING MODE DAMPING WITH AND WITHOUT STALL EFFECTS IN FORWARD FLIGHT FOR HIGH SHAFT TILT ANGLES FOR θ_o=0°

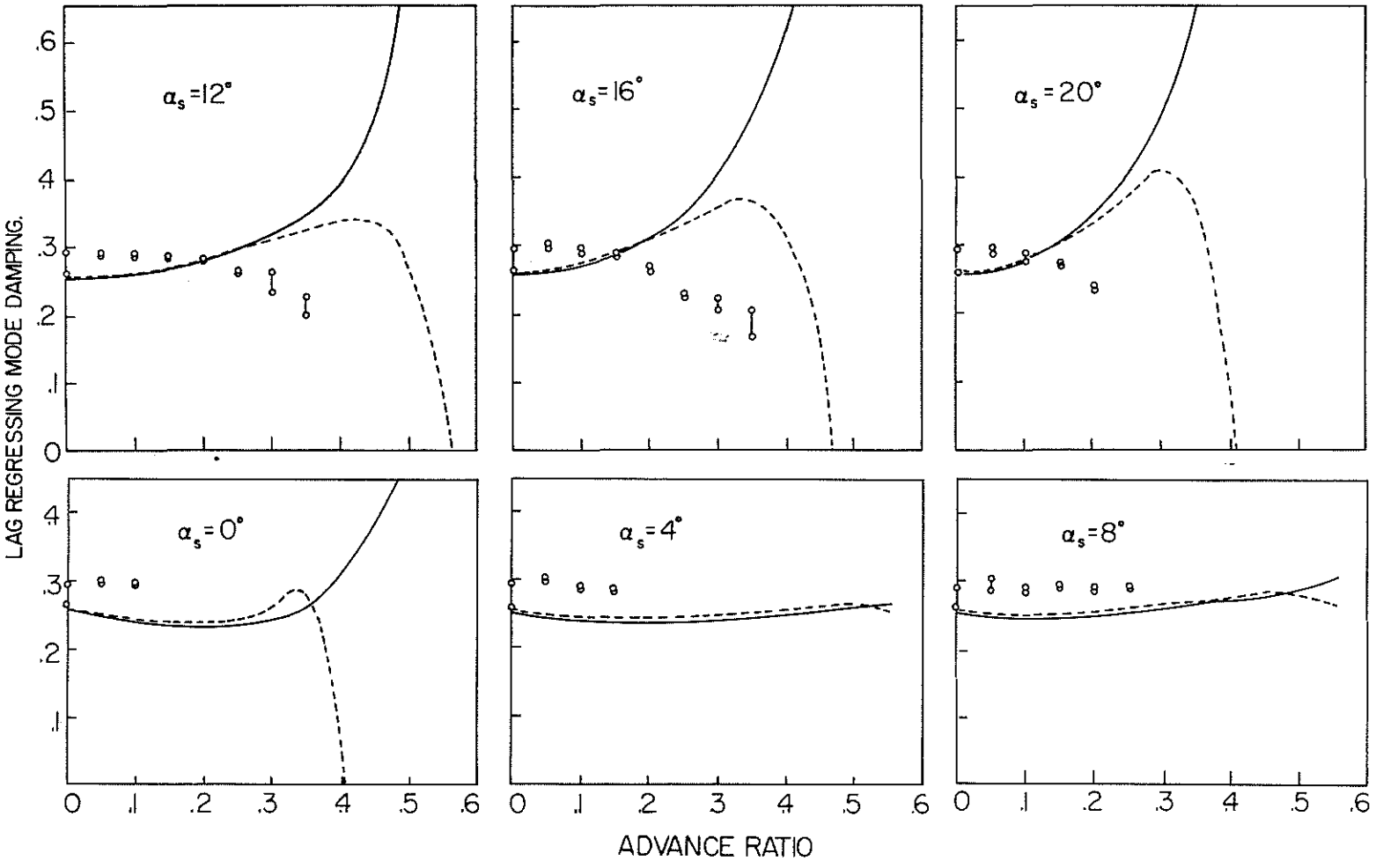

FIG. 7 CORRELATION OF LAG REGRESSING MODE DAMPING WITH AND WITHOUT STALL EFFECTS IN FORWARD FLIGHT, θ_o = 3°

character of this reduction is quite different. For small values of shaft-tilt angle α_s° (≤ 8), the data is available for $\mu \leq .25$ and stall is hardly an issue. The minor differences between the two theories are due to nonlinear drag in substall. That the stall theory shows sudden decrease in damping at $\mu \approx .4$ for $\alpha_s^\circ = 0$ is likely due to sudden increase in stall effects, as seen from the stall plots in figure 5 for $\theta_0^\circ = 3$ and $\alpha_s^\circ = 0$. Further, as seen from figure 7 for $\alpha_s^\circ = 0$, 4, and 8, the difference between theory and data remains nearly the same as it was in hover. According to an earlier study, that difference was found not to be associated with nonuniform steady inflow (more discussion on this difference later in figure 13). For higher shaft-tilt angles ($\alpha_s^\circ \geq 12$) in figure 7 the stall effects are negligible for the following three ranges of data: $\mu \leq .275$, $\alpha_s^\circ = 12$; $\mu \leq .225$, $\alpha_s^\circ = 16$; and $\mu \leq .175$, and $\alpha_s^\circ = 20$. That is, less than 10-12% of the disk is in stall and there is negligible difference between the two theories. For the remaining three ranges of data with $\alpha_s^\circ \geq 12$, stall effects become increasingly important with increasing μ and α_s. For example, at $\mu = .35$ and $\alpha_s^\circ = 16$, nearly 25% of the disk is in stall. The stall theory substantially differs from the linear theory but still does not correlate well with the data.

Figure 8 shows the correlation for the six-degree collective case. Only a limited amount of data are available ($\mu \leq .15$) and stall is not an issue here (less than 10% of the disk experiences stall for the entire set of data, also see figure 5 for $\theta_0^\circ = 6$ and $\alpha_s^\circ = 16$). The behaviour of the theories relative to each other remains essentially as it was for the 3° collective case.

The predictions from the stall theory, as presented earlier, include the total stall effects of lift and drag. It is instructive to estimate how much of that total is due to nonlinear lift and how much, due to nonlinear drag. This question is addressed in figure 9 for hovering and in figure 10 for forward flight. The hovering case has eight degree collective treated earlier in figure 3, and substall conditions are present throughout ($\alpha \approx 4^\circ$ at .7R). We have shown predictions for four cases---linear lift and drag in combination with nonlinear local lift and drag -- as identified in the figure. Given the substall conditions, the nonlinear lift characteristics have no impact on the predictions. As expected, the predictions from the nonlinear lift-and-drag theory (stall theory) merges with those from the linear-lift and nonlinear-drag theory. The same is true of the other two predictions from the nonlinear-lift and constant-drag theory and the linear-lift and constant-drag theory (linear theory). Thus the relevant ingredient below stall is nonlinear drag,

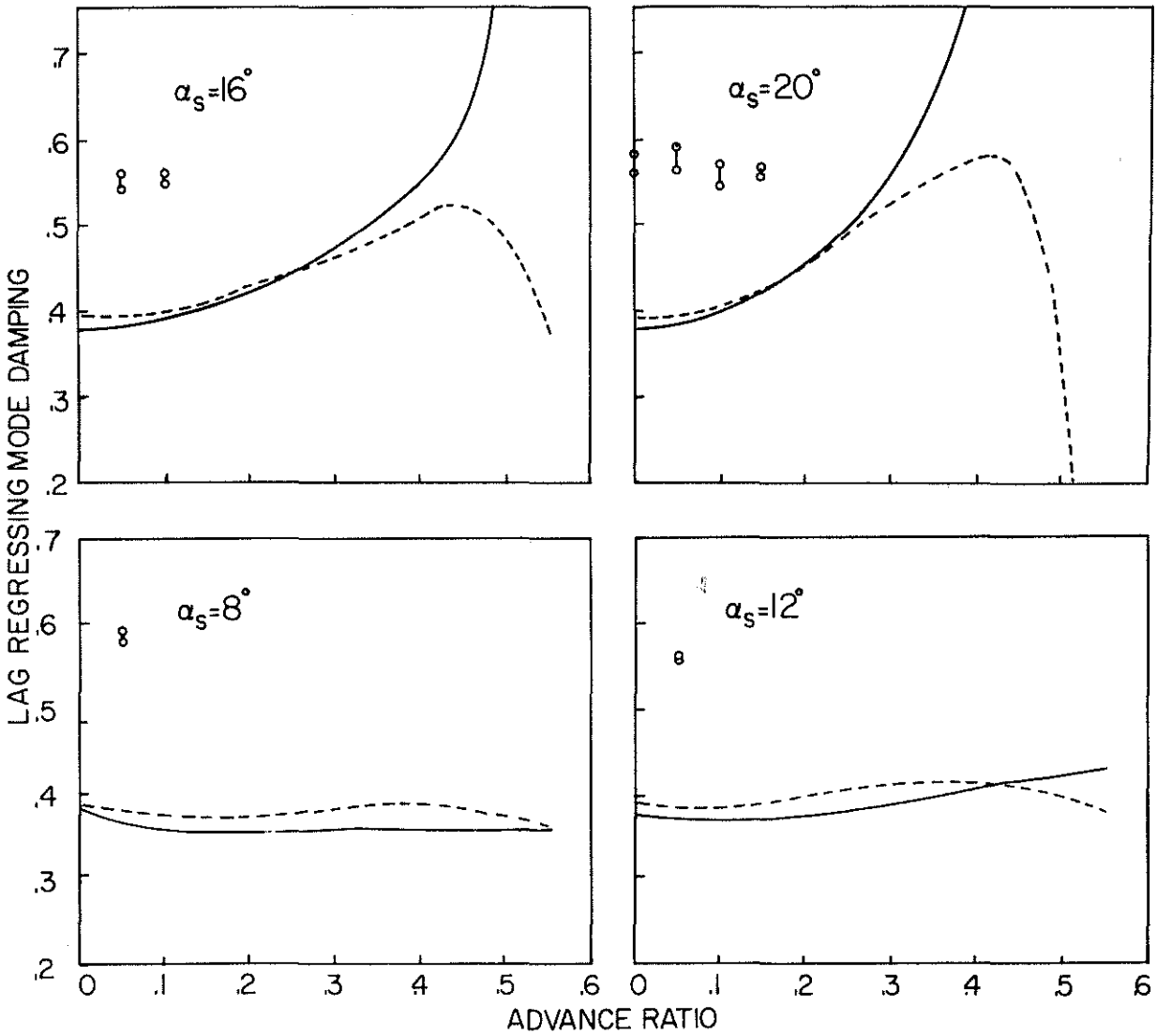

FIG 8 CORRELATION OF LAG REGRESSING MODE DAMPING WITH AND WITHOUT STALL EFFECTS IN FORWARD FLIGHT FOR θ_0=6°

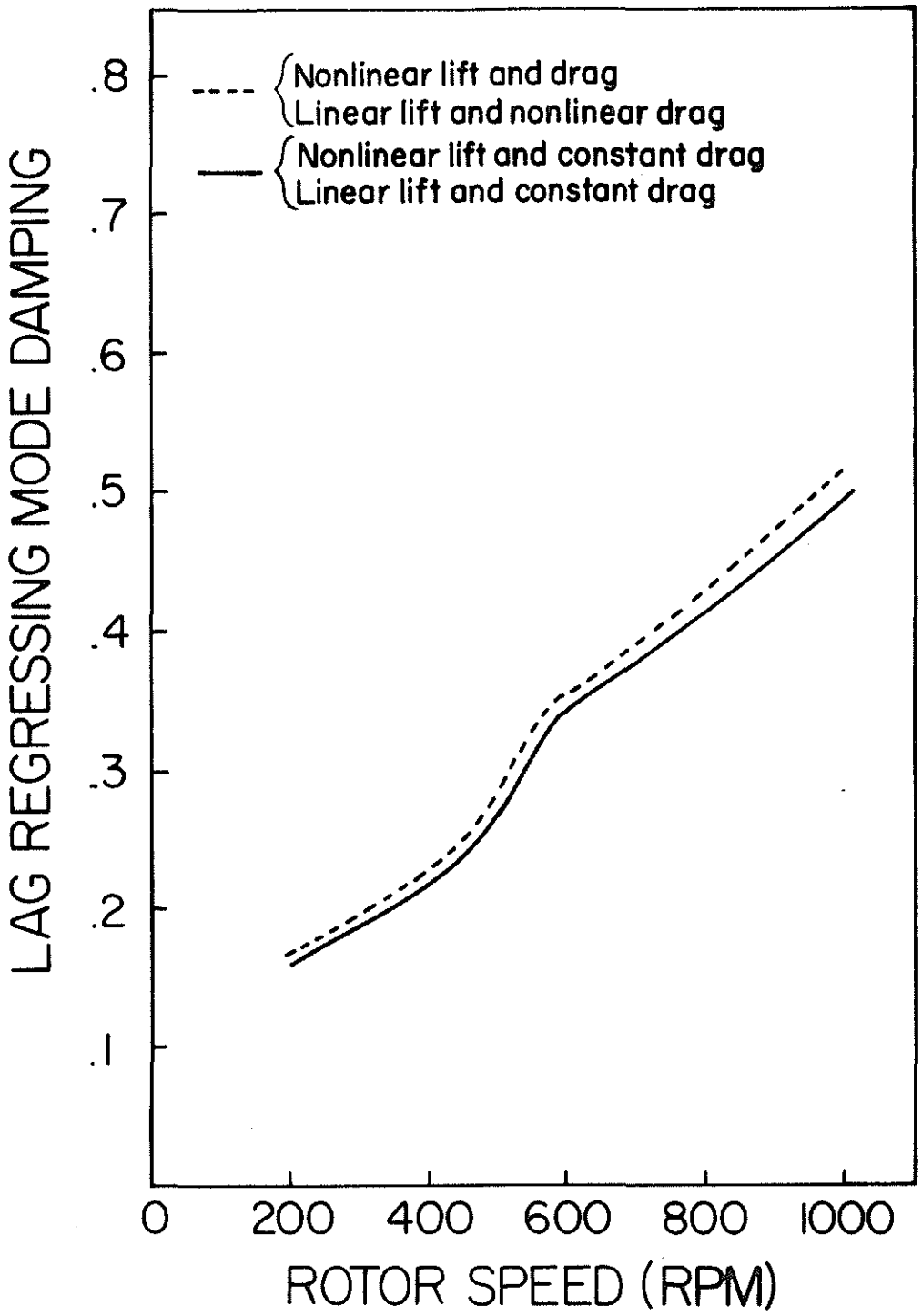

FIG.9 ISOLATION OF THE EFFECTS OF NONLINEAR LIFT AND DRAG IN HOVER FOR $\theta_0 = 8.^\circ$

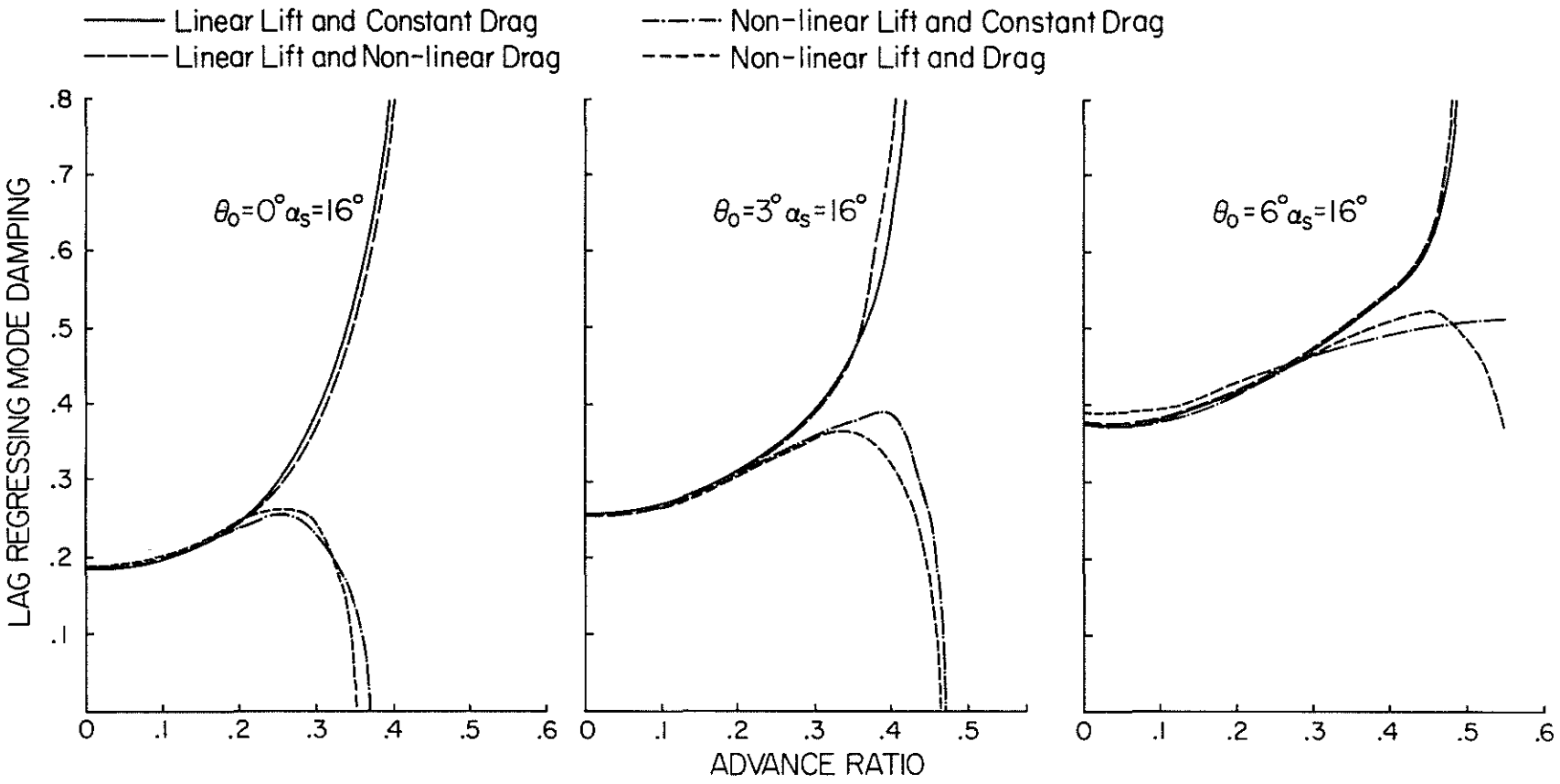

FIG. 10 ISOLATION OF THE EFFECTS OF NON-LINEAR LIFT AND DRAG IN FORWARD FLIGHT ($\alpha_s=16°$)

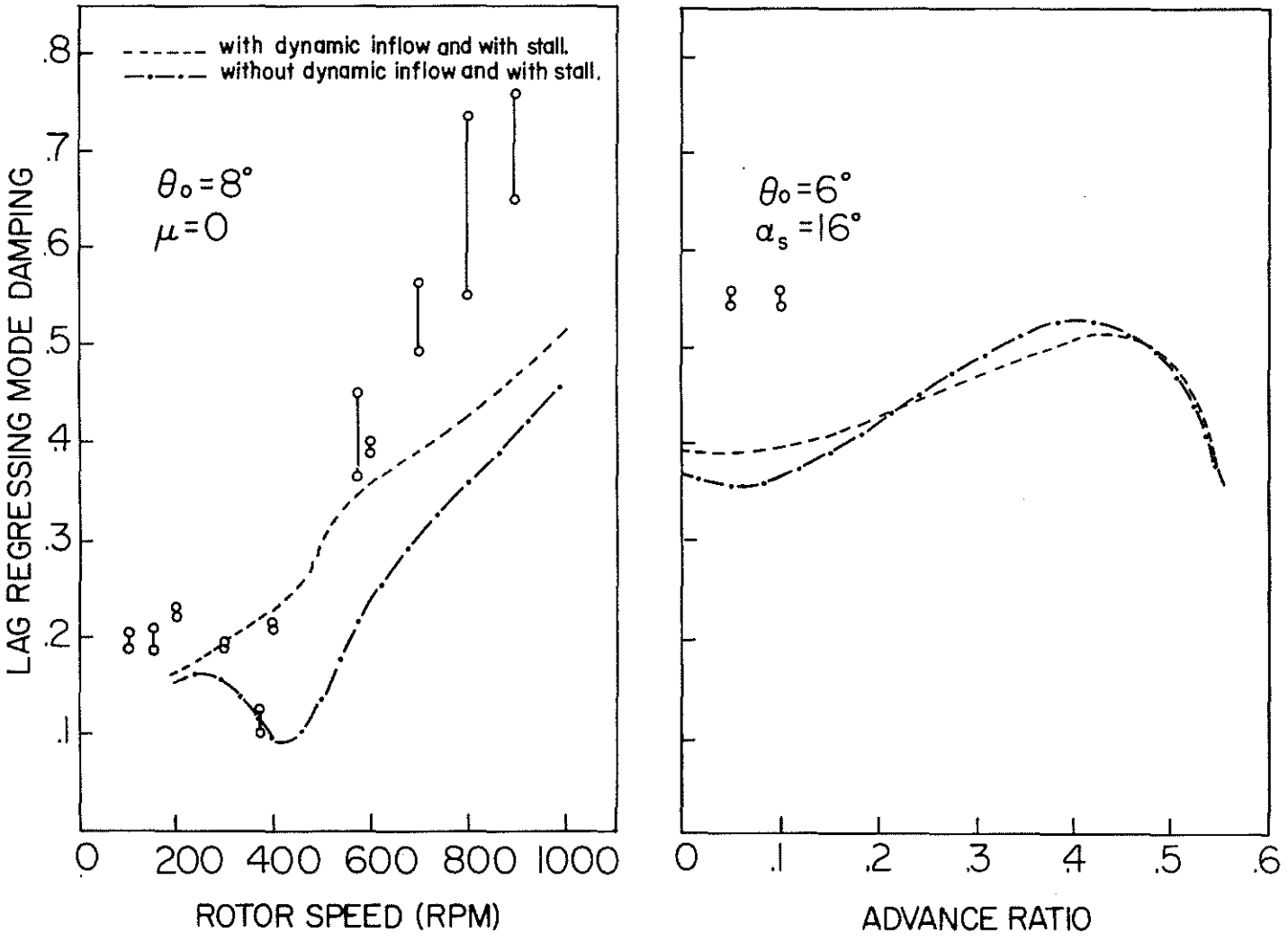

FIG.11 EFFECTS OF DYNAMIC INFLOW ON LAG REGRESSING MODE DAMPING WITH STALL.

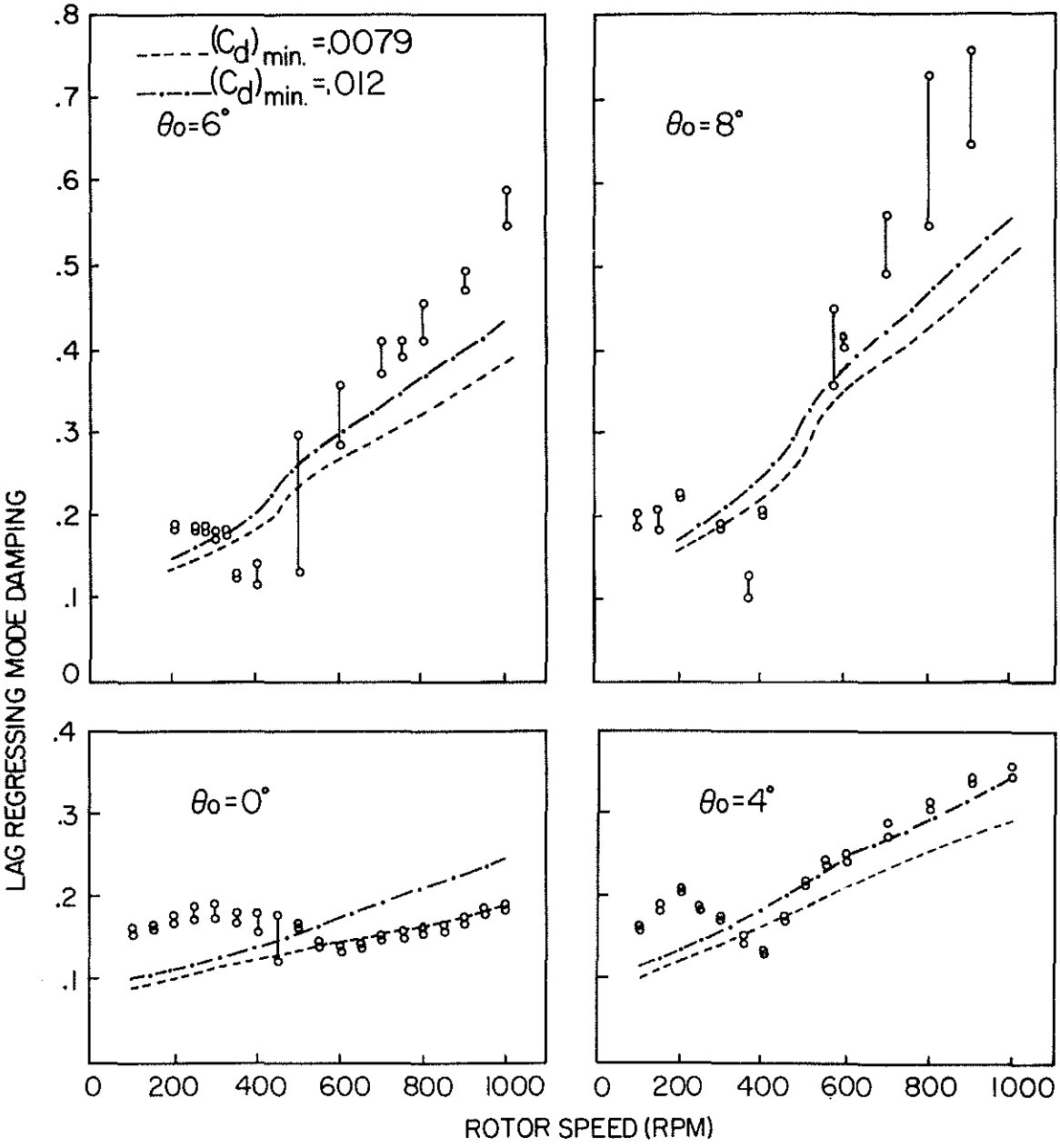

FIG.12 LAG REGRESSING MODE DAMPING WITH $(C_d)_{min}$ = .0079 AND .012 IN HOVER WITH STALL

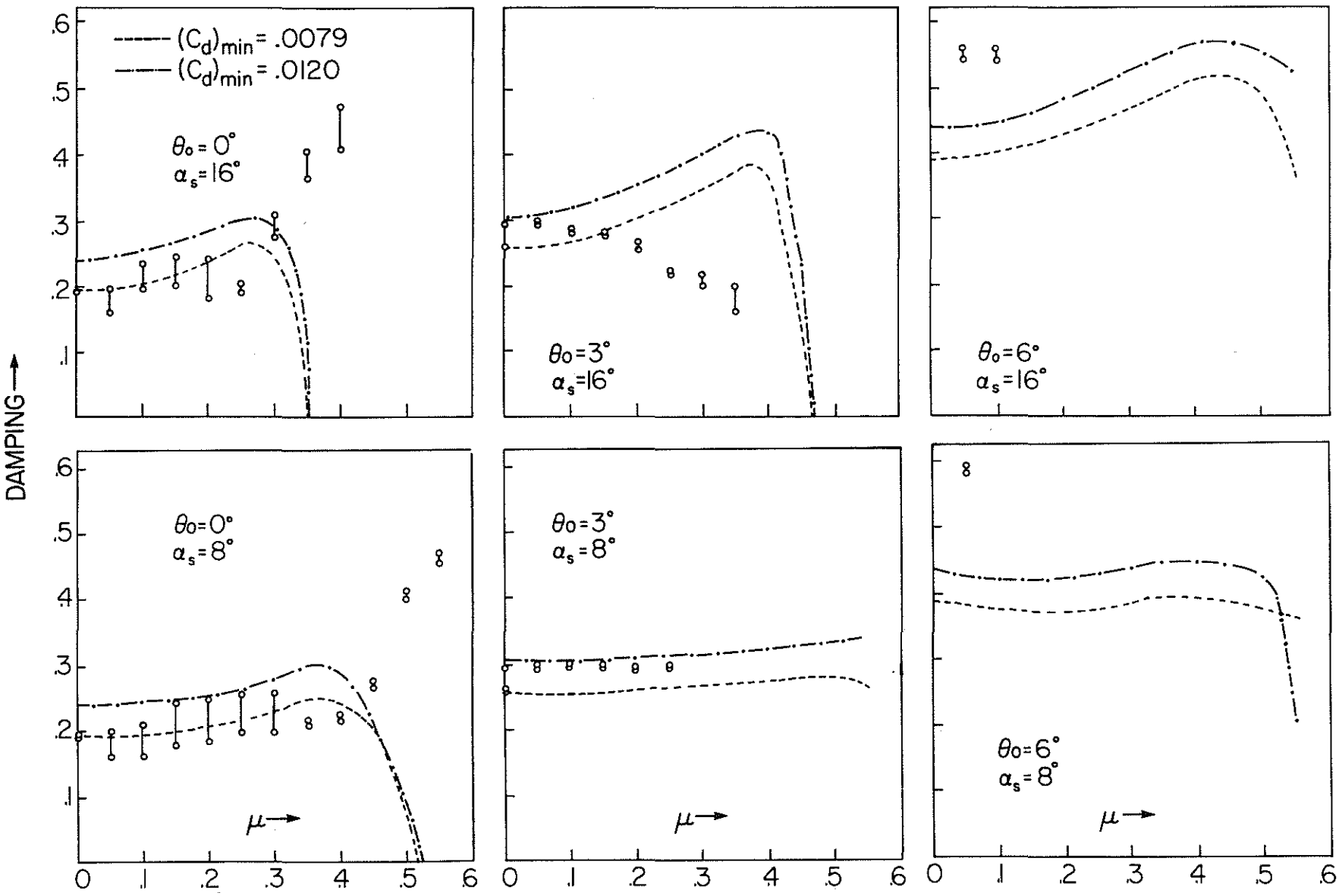

FIG. 13 LAG REGRESSING MODE DAMPING WITH (Cd)min=.0079 AND $(C_d)_{min}$ = .012 IN FORWARD FLIGHT.

6-2-24

although for the specific case in figure 9, its impact is not appreciable. Nevertheless, the simplicity of the hovering case lays the ground work for the more demanding forward-flight case taken up next.

Figure 10 shows the predictions for the same four combinations of lift and drag characteristics treated for the hovering case and these combinations are identified in figure 10. We have included all the three cases with θ_0° = 0, 3, and 6 as treated earlier (figures 4, 6, 7 and 8). In substall, the predictions are as expected. However, when stall becomes an issue, that is, when more than 10-12% of the disk is in stall (θ_0° = 0, $\mu \geq 0.225$, θ_0° = 3, $\mu \geq .225$ and θ_0° = 6, $\mu \geq .3$) the trends of the predictions are extremely interesting, particularly of the predictions from the nonlinear-lift and constant-drag theory. It is seen that the key ingredient is nonlinear lift (and not nonlinear drag) that affects the prediction qualitatively (increasing or decreasing damping with increasing μ).

In figure 11, we address the question of how much better is the stall theory with dynamic inflow when compared to the stall theory without dynamic inflow. In hover dynamic inflow improves the correlation consistently and throughout. In forward flight the impact of dynamic inflow is negligible and a typical example is shown in figure 11 for θ_0° = 6 and α_s° = 16.

Finally, in figures 12 and 13, we discuss the sensitivity of the predictions to the assumed values of c_d (α = 0) or $c_{d,min}$ values. While figure 12 refers to the hovering conditions for four values of the collective pitch setting (as in figure 3), figure 13 refers to the forward flight conditions for a typical cross section of the data in forward flight, as in figures 6,7, and 8. In substall, the higher value .012 gives better overall correlation both in hover and forward flight. This covers all the hovering data and part of the data in forward flight as discussed earlier. When more than 10-12% of the disk is in stall, we know from figure 11 that the predictions are qualitatively affected by nonlinear local lift and not by nonlinear local drag. This is well borne out by the results in figure 13 which shows that the qualitative aspects of the prediction in stall are not sensitive to reasonable changes in the assumed $c_{d,min}$ values.

CONCLUDING REMARKS

1. When less than 10-12 percent of the disk is stalled the linear and non linear theories give nearly the same results, with the nonlinear theory marginally better. When 10-20% of the disk is in stall, the nonlinear theory may

slightly improve the correlation. However only a limited number of data are involved in this range and this improvement is not conclusively demonstrated.

2. For highly stalled cases in forward flight, when more than about 25 percent of the disk is stalled, the stall theory differs markedly from the linear theory, but neither theory does well. However, the linear theory seems to be "qualitatively accurate" for $\theta = 0°$. That the linear theory shows the qualitative accuracy is peculiar since appreciable stall effects should be expected. That the highly stalled, high advance ratio cases are not well predicted by the nonlinear theory perhaps indicates dynamic stall effects.

3. In hover, the data is in substall, and the difference between the stall theory and data increases with increasing Ω and θ_0. This difference is not associated with nonlinear local drag characteristics. The correlations were conducted for $C_{d,min} = 0.0079$ and 0.012. The latter higher value gives better correlation in hover, and in forward flight in substall. Under stall conditions of forward flight, the qualitative aspect of the correlation is not sensitive to perturbations in $C_{d,min}$ values.

4. For stall conditions of forward flight, the key ingredient is nonlinear local lift coefficient which qualitatively changes the prediction when compared with the predictions from the linear theory, and from the theory with linear-lift and nonlinear-drag characteristics. Further, while the theory with nonlinear-lift and constant-drag characteristics is close to the stall theory, the theory with linear-lift and nonlinear-drag characteristics is close to the linear theory.

5. Quasi-steady stall theory with dynamic inflow improves the correlation somewhat in hover but the forward flight results, while qualitatively very different than the linear theory results, do not overall show improved correlation with the data.

ACKNOWLEDGEMENT

We are grateful to Messrs. Robert Ormiston and William Bousman for their encouragement and extensive comments. We also thank Mrs. Sylvia Bone for her hard work and persistence in word processing this paper. This work is sponsored by the U. S. Army Aeroflightdynamics Directorate, NASA-Ames Research Center under grant no. NCC 2-361, and by the U. S. Army Research Office under grant no. DAAL03. The view, opinions and/or findings contained in this report

are those of the authors, and should not be construed as an official Department of the Army position, policy, or decision, unless so designated by other documentation.

REFERENCES

1. Gaonkar, G.H., McNulty, M.J. and Nagabhushanam, J., "An Experimental and Analytical Investigation of Isolated Rotor Flap-Lag Stability in Forward Flight", NAS2-361, U.S. Army Aeroflightdynamics Directorate, July 1986, (11th European Rotorcraft Forum, London, England, September 10-13, 1985, Paper No. 66, Revised).
2. Bousman, W.G. and Ormiston, R.A., "A Study of Stall Induced Flap-Lag Instability of Hingeless Rotors", 29th Annual National Forum of the American Helicopter Society, Washington, D.C., May 1973, Preprint No. 730.
3. Bousman, W.G., Sharpe, D.L. and Ormiston, R.A., "An Experimental Study of Techniques for Increasing the Lead-Lag Damping of Soft Inplane Hingeless Rotors", 32nd Annual National V/STOL Forum of the American Helicopter Society, Washington, D.C., May 1976, Preprint No.1035.
4. Jacobs, E.N. and Sherman Albert, Airfoil Section Characteristics as Affected by Variations of the Reynolds Number, NACA Report No. 586, 1937.
5. Critzos, C.C., Heyson, H.H., and Boswinkle, R.W., Aerodynamic Characteristics of NACA 0012 Airfoil Section at Angles of Attack from 0 to 180, NACA Technical Note No. 3361, 1955.
6. Nagabhushanam, J., Gaonkar, G. H., and Reddy, T. S. R., "Automatic Generation of Equations for Rotor-Body Systems with Dynamic Inflow for A Priori Ordering Schemes", Seventh European Rotorcraft Forum, Garmisch-Partenkirchen, Federal Republic of Germany, September 8-11, 1981, Paper No. 37.
7. Nagabhushanam, J. et al. Users' Manual for Automatic Generation of Equations of Motion and Damping Levels for Some Problems of Rotorcraft Flight Dynamics, R & R Report, HAL-IISC Helicopter Training Program, Indian Institute of Science Bangalore, India, October, 1984.